Asociación Argentina
de Mecánica Computacional

Mecánica Computacional Vol XXX, págs. 3385-3393 (artículo completo)
Oscar Möller, Javier W. Signorelli, Mario A. Storti (Eds.)
Rosario, Argentina, 1-4 Noviembre 2011

HEMODYNAMIC CHARACTERISTICS AT ANTERIOR COMMUNICATING ARTERY BEFORE ANEURYSM INITIATION USING PATIENT-SPECIFIC FINITE ELEMENT BLOOD FLOW SIMULATIONS

Marcelo A. Castro [a, c], **Christopher M. Putman** [b], **Juan R. Cebral** [c]

[a] *CONICET, Grupo de Investigación y Desarrollo en Bioingeniería, Facultad Regional Buenos Aires, UTN, Medrano 951, Buenos Aires, Argentina, marcelo.a.castro@gmail.com, http://sites.google.com/site/marceloadriancastro*

[b] *Department of Interventional Neuroradiology, Inova Fairfax Hospital, 3300 Gallows Rd., Falls Church, Virginia, USA*

[c] *Department of Computational and Data Sciences, George Mason University, 4400 University Blvd., Fairfax, Virginia, USA, jcebral@gmu.edu, http://cfd.gmu.edu/~jcebral*

Keywords: Cerebral aneurysms, Anterior communicating artery, Numerical simulations

Abstract. The anterior communicating artery (AComA) is a unique vascular location that receives blood from two sources of inflow and redistributes it toward the anterior part of the brain through two efferent arteries. It is widely accepted that complexity in the flow pattern is associated with the high rate of aneurysm formation in that location observed in large studies. A previous computational hemodynamic study showed a possible association between high maximum intraaneurysmal wall shear stress (WSS*)* at the systolic peak with rupture in a cohort of AComA aneurysms. In another study it was observed a connection between location of aneurysm blebs and regions of high WSS in models where blebs were virtually removed. The purpose of this work is to study associations between hemodynamic patterns and AComA aneurysm initiation by comparing hemodynamics between the aneurysm models and the normal model where the aneurysm was computationally removed. Vascular models of both right and left circulation were independently reconstructed from three-dimensional rotational angiography images using deformable models after image registration of both images, and later fused using a surface merging algorithm. Afterwards, the geometric models were used to generate high-quality volumetric finite element grids composed several million tetrahedral elements with an advancing front technique. For each patient the second anatomical model was created by digitally removing the aneurysm. It was iteratively achieved by applying a Laplacian smoothing filter and remeshing the surface. Finite element blood flow numerical simulations were performed for both the pathological and normal models under the same flow conditions. Personalized pulsatile flow conditions were imposed at the inlets of both models with use of the Womersley solution. The Navier-Stokes equations were numerically integrated by using a fully implicit finite-element formulation. From analysis of WSS distributions it was observed that aneurysms initiated in regions of high and moderate WSS in the counterpart normal models. Adjacent or close to those regions, low WSS portions of the arterial wall were not affected by the disease. These results are in line with previous reported observations at other vascular locations.

1 INTRODUCTION

Cerebral aneurysms are pathological dilatations of the arterial wall that occur at or near arterial bifurcations. Most cerebral aneurysms appear in the Circle of Willis, located at the base of the brain. The anterior communicating artery (AComA) is a unique vascular location that ideally receives blood from two sources of inflow and redistributes it toward the anterior part of the brain through two efferent arteries (Perlmutter et al.,1976). However, aneurysms of the AcomA complex are more likely to have hypoplastic A1 segments (Kasuya el al., 1999) or to have exclusive filling angiographically from one A1 segment in up to 78% cases (Charbel et al., 1991). Those AComA aneurysms receiving blood from both A1 segments have flow patterns dependent of individual flow rates and wave forms, which may result in regions of elevated wall shear stress (WSS) that change their locations during the cardiac cycle (Castro et al., 2006a). It is widely accepted that complexity in the flow pattern is associated with the high rate of aneurysm formation observed in large studies (Brilstra et al., 1990; Horiuchi et al., 2005; Leipzip et al., 2005).

There is agreement about the role of wall shear stress (WSS) in the formation, growth and ultimately rupture of cerebral aneurysms (Nakatani et al., 1991; Crompton et al., 1996). A previous computational hemodynamic study showed a possible association between high maximum WSS at the systolic peak with rupture in a cohort of AComA aneurysms (Castro et al., 2009a). In that study ruptured aneurysms had in average as much as twice maximum WSS as in the unruptured group. This result is in line with a previous study where AcomA aneurysms were experimentally produced in hypertensive rats by unilateral ligation of the common carotid artery (Hashimoto et al., 1980). Similar findings were reported for terminal aneurysms including unilateral AComA aneurysms (Castro et al., 2009b). Additionally, in a large study including 210 cerebral aneurysms at different locations it was found a statistical significant association between rupture and WSS distributions with elevated maximum WSS, high flow concentration and small impingement size (Cebral et al., 2011). Cebral et al. also showed a connection between location of aneurysm blebs and regions of high WSS in models where blebs were virtually removed (Cebral et al., 2010). In another study, it was presented a relationship between rupture, and coexistence of high WSS and high positive spatial WSS gradient, observed in three-patient scanned before and after aneurysm formation (Kulcsar et al., 2011). The normal vasculature had been incidentally imaged when investigating other pathologies. Although other investigators reported possible associations between low shear stress and either rupture (Jou et al., 2008; Shojima et al., 2004) or blister formation (Shojima et al., 2010), most experimental, clinical and numerical evidence suggest a connection between high WSS values and aneurysm formation. Particularly, the 20 vascular models harboring aneurysms in the middle cerebral artery reconstructed in Shojima et al., 2004, considered a limited portion of the parent artery, neglecting important features of the vascular geometry that resulted in a simplified simulated blood flow. Later, it was demonstrated that such simplifications significantly alter intra aneurysmal flow patterns (Castro et al., 2006c).

The purpose of this work is to study associations between hemodynamic patterns and aneurysm initiation by comparing AComA hemodynamics between the original aneurysm model and the vascular model where the aneurysm was computationally removed. Patients included in this study were not scanned before aneurysm formation. Therefore, there is no evidence to determine whether or not the original vascular configurations were affected by the disease. In this preliminar study, in order to minimize the effects of the reconstruction method, only a selected group of patients whose aneurysms affected a limited region of the AComA and the parent artery were considered.

2 METHODS

2.1 Angiographic images and vascular modeling

Bilateral rotational scans were obtained to visualize both avenues of flow into the anterior communicating artery (AcomA) aneurysm using a Philips Integris System (Philips Medical Systems, Best, The Netherlands) in three selected patients with cerebral aneurysms in the AComA. Each 8-second acquisition consisted in 120 projections obtained during a 180° rotation, which were reconstructed into a 3D dataset of 128^3 voxels covering a field of view of 54.02 mm on a dedicated workstation. The voxel resolution was therefore 0.422 mm. These data were exported into a PC for mathematic vascular modeling using a previously presented methodology (Yim et al., 2002; Cebral et al., 2005; Castro et al., 2009a).

Vascular models of both right and left circulation were independently reconstructed using deformable models (Castro et al., 2006b) after rigid registration of both images. Independent models were fused using a surface merging algorithm (Cebral et al., 2001). Models were smoothed, and vessel branches were truncated and extruded along the vessel axis. The geometric models were then used to generate high-quality volumetric finite element grids composed of tetrahedral elements with an advancing front technique (Löhner et al., 1996a; Löhner et al., 1996b; Löhner et al., 1997). Element size was adjusted in order to approximately maintain the same number of elements in both large and small arteries. A minimal mesh resolution of 0.16 mm was prescribed for internal carotid arteries, which resulted in grids containing up to 2.5 million tetrahedra. Afterwards, a normal model was reconstructed for each case by digitally removing the aneurysm in the original models, starting from the smaller high curvature structures. It was iteratively achieved by applying a Laplacian smoothing filter and remeshing the model, in order to avoid high distortions in triangle aspect ratio and size due to the strong deformations required to remove the aneurysm. Aneurysm boundary points (neck of the aneurysm) were fixed in order for the Laplacian filter not to shrink the model beyond the affected region (Cebral et al., 2010).

2.2 Blood flow numerical simulations

Finite element blood flow numerical simulations were performed for both the original and the pre-aneurysm models under the same flow conditions. Blood was modeled as an incompressible Newtonian fluid with attenuation 1.0 g/cm3 and viscosity 0.04 Poise. The governing equations were the unsteady Navier-Stokes equations in 3D (Mazumdar, 1992). Vessel walls were assumed rigid, and no slip boundary conditions were applied at the walls. Pulsatile flow conditions derived from PCMR measurement in healthy subjects were imposed at the inlet of the models. Flow waveforms were scaled with the inlet area to achieve a mean WSS of 15 dyne/cm^2 at the inflow boundary of each model. This choice is consistent with studies relating vessel area and flow rates in internal carotid and vertebral arteries (Cebral et al., 2008), as well as with the principle of minimal work expressed by Murray's law (Sherman, 1981). Fully developed pulsatile velocity profiles were prescribed with use of the Womersley solution (Womersley, 1955; Taylor et al., 1998). Assuming that all distal vascular beds have similar total resistance to flow, traction-free boundary conditions with the same pressure level were applied at outlet boundaries. The Navier-Stokes equations were numerically integrated by using a fully implicit finite-element formulation (Cebral et al., 2005). Two cardiac cycles using 100 time-steps per cycle were computed, and all of the results reported correspond to the second cardiac cycle.

2.3 Data reduction and analysis

Maps of WSS magnitude were created to visualize the distribution of shear forces on the aneurysm wall, as well as parent and efferent vessels. All elements in the normal model whose distance to the aneurysm model was greater than two element sizes were marked. Those elements are located in a region of original arterial wall where the aneurysm started to form. WSS distributions and histograms were studied over that region, and WSS values were compared to those typical values in the surrounding region.

3 RESULTS

Two cases were selected from our data base. For each of them, model A (without aneurysm) and model B (with aneurysm) were created. The aneurysm information, including both right and left internal carotid artery cross sectional area, aneurysm neck area, maximum perpendicular and parallel distance and aspect ratio, is shown in Table 1.

Original models for both cases are shown in Figure 1a,b, while models after digital intervention to remove the aneurysm from the original models are shown in Figure 1c,d. WSS distributions in model A along with the mesh corresponding to model B, for both Case #1 and Case #2, are shown in Figure 1e and figure 1f, respectively.

For Case #1 a high WSS region with a peak of 150 dyne/cm^2 is observed in the AcomA, surrounded by a larger region with moderate WSS values ranging between 50 dyne/cm^2 and 150 dyne/cm^2. Comparison between both models shows that the aneurysm started to form in the high WSS region. Lower WSS values of 25 dyn/cm^2, in average in the surrounding region are observed.

For patient #2, two disconnected high WSS regions with peak values of 75 dyne/cm^2 and 50 dyne/cm^2 were observed, exhibiting an intermediate region with moderate WSS values. The extended area affected by the aneurysm covered those three regions. Adjacent to them there is a low WSS portion of the feeding vessel with values of 25 dyne/cm^2 in average, and no higher than 40 dyn/cm^2.

From WSS distribution, the region of model A corresponding to the inner part of the neck (internal) was used to compute a histogram, which was compared to the histogram for the region outside the inner region (external). Figure 2a,b shows those histograms. For both Case #1 and Case #2, histograms of internal and external region are hardly overlapped. Most high WSS values appear in the internal region while surrounding regions are exposed to low WSS values. For Case #1, the internal and external regions had areas of 0.035 cm^2 and 0.019 cm^2, respectively, while those for Case #2, were 0.114 cm^2 and 0.140 cm^2, respectively.

Case #	Area ICA left (cm^2)	Area ICA right (cm^2)	Anuerysm neck area (cm^2)	Max dist $\perp$ (cm)	Max dist $\parallel$ (cm)	AR
1	0.116	0.140	0.035	0.90	0.50	1.80
2	0.251	0.177	0.114	0.57	0.44	1.29

Table 1: a) case number; b) cross-sectional area of the left ICA at the inflow; c) cross-sectional area of the right ICA at the inflow; d) maximum length of the aneurysm perpendicular to the vessel; e) maximum length of the aneurysm parallel to the vessel; f) aspect ratio of aneurysms.

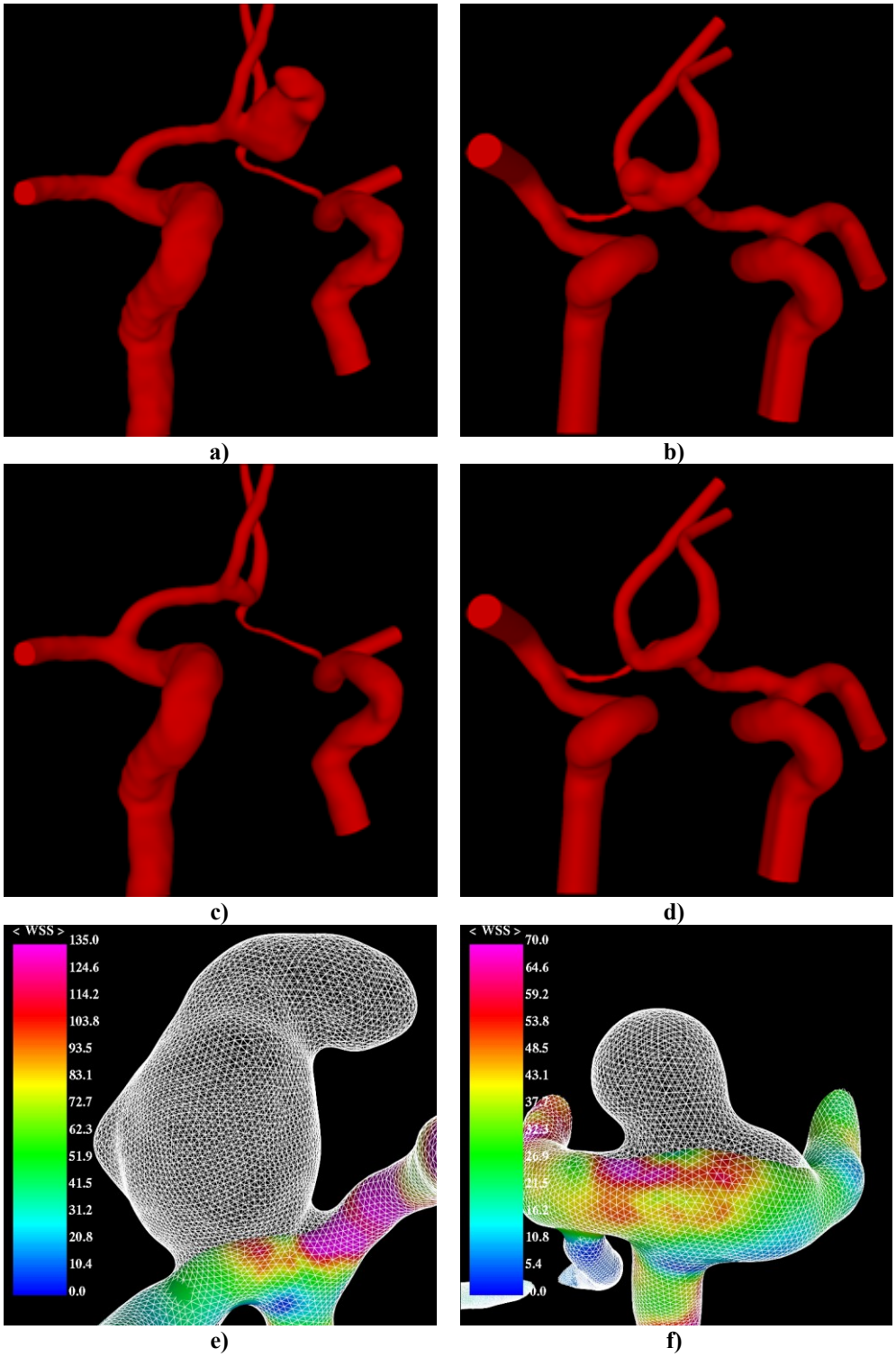

Figure 1: original vascular models after merging of right and left models for Case #1 (a) and Case #2 (b); (b) vascular models after digital intervention to remove AComA aneurysm for Case #1 (c) and Case #2 (d); spatial distributions of the absolute value wall shear stress at the systolic peak in models after digital intervention, overlapped with the mesh corresponding to the original models, for Case #1 (e) and Case #2 (f).

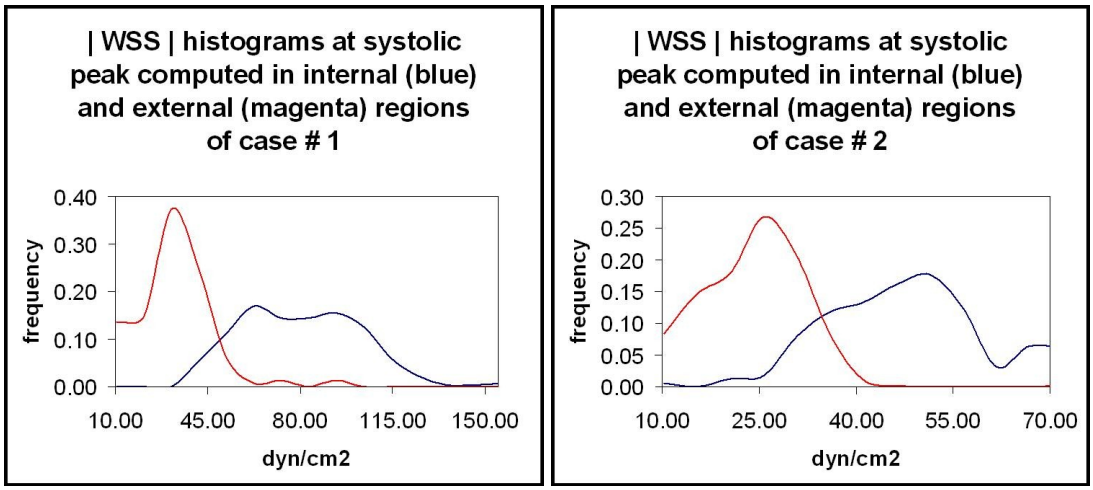

a) **b)**

Figure 2: histogram of WSS values in model A for Case#1 (a) and Case #2 (b). Blue curves correspond to those computed in the internal regions, while magenta curves corresponds of those for the external ones. Internal areas for Cases #1 and #2 were 0.035 cm^2 and 0.114cm^2, while external ones were 0.019 cm^2 and 0.140 cm^2.

4 DISCUSION

The purpose of this work is to extend a previous developed methodology for patient-specific image-based computational hemodynamics studies of vascular cerebral networks harboring intracranial aneurysms (Cebral et al., 2005; Castro et al., 2006a; Castro et al. 2009a; Cebral et al., 2010). Reconstruction of computational models from 3DRA images of systems fed by more than one parent artery, typical situation at several locations in the Circle of Willis, pose an additional complication. A methodology to overcome this limitation, based on multiple images acquired with contrast injections at different locations was previously presented (Castro et al., 2006a). That methodology was later used to study in detail hemodynamic characteristics of anterior communicating artery aneurysms in a set a patient-specific cases. First, it was observed that bilateral AComA aneurysm (those ACom arteries that have both A1 segments of the anterior cerebral artery) may hemodynamically behave as unilateral AComA aneurysms (those ACom arteries with an hypoplastic A1 segment). The ratio observed in our computational simulations was in close agreement with previously data reported from radiological examinations. Additionally, it was found that AComA aneurysms fed by just one A1 artery, had hemodynamic characteristics that remained unchanged when changes in the ICA flow rates or shifts in the waveforms were imposed (Castro et al., 2006b). Bilateral systems, however, showed changes in the WSS distributions, particularly, the location where the maximum WSS values appeared. Therefore, a uniform criterion to scale waveforms with the inlet area to achieve a mean WSS of 15 dyne/cm^2 at the inflow boundary of each model was chose. This choice is consistent with studies relating vessel area and flow rates in internal carotid and vertebral arteries, as well as with the principle of minimal work expressed by Murray's law (Sherman, 1981).

Later, a cohort of 26 patients with AComA aneurysms, both bilateral and unilateral, was investigated. Flow patterns were classified according to the way in which the inflow jet splits at the aneurysm neck. The maximum rupture rate was found in those aneurysms having one of the inflow jets impacting and splitting in the aneurysm neck, producing high WSS values. It was also found that the maximum intra aneurysmal WSS at the systolic peak averaged over the ruptured group was roughly as much as twice as that over the unruptured. That may indicate that there is a possible association between high WSS an aneurysm rupture

(Castro et al. 2009a). The same result was found in cohort of terminal aneurysms at different vascular locations in the brain (Castro et al., 2009b).

In a previous study Cebral et al. also showed a connection between location of aneurysm blebs and regions of high WSS in models where blebs were virtually removed (Cebral et al., 2010). An extension of that methodology is applied in the work presented in this paper. A combination of mesh smoothing using Gaussian filters and remeshing over the aneurysm region limited by the neck boundary was applied to remove the AComA aneurysm.

From the results obtained in the test cases, aneurysms started to form in a region of high and moderate WSS values, compared to low WSS values in surrounding regions. This observation is in line with previously reported results from patient-specific blood flow finite element simulations at other vascular locations (Castro et al., 2009a, Castro et al., 2009b, Cebral, 2010). This trend will have to corroborated by larger studies, which also include other hemodynamic quantities. Future works will also study in detail differences in hemodynamic patterns between unilateral and bilateral aneurysms before and after aneurysm initiation.

The methodology has some potential limitations. The digital removal of AComA aneurysms may be not accurately applied to large aneurysms with wide necks where the original vasculature may not be easily reconstructed. Ford et al. presented an approach to digital removal of saccular aneurysms (Ford et al., 2009). Although the methodology presented there is automatic and may be helpful to process large amount of data, it may generate simplified bifurcation geometries due to the centreline based reconstruction. That may affect WSS computation in models where aneurysms where removed from those locations. The best scenario would be to analyze images after and before aneurysm initiation. Images before aneurysm formation are usually acquired by chance when the patients is screened because of another pathology or aneurysms at other locations (Kulcsar et al., 2011), therefore they can not be used to carry out a large study. Another potential limitation is the use non-patient-specific flow rate waveforms imposed at the inlet of our models. However, this limitation is suffered by most computational studies since flow rate measurements are not routinely acquired in clinical evaluations. This limitation is partially overcome by WSS normalization at inflow segments, which allows comparison between different models. Other model assumptions had limited impact on aneurismal hemodynamics, as it was shown in previous works (Cebral et al., 2005).

REFERENCES

Brilstra, E.H., Rinkel, G.J., van der Graff, Y., Treatment of intracranial aneurysms by embolization with coils: a systematic review. *Stroke*, 30:470–476, 1990.

Castro, M.A., Putman, C.M., Cebral, J.R., Patient-Specific Computational Fluid Dynamics Modeling of Anterior Communicating Artery Aneurysms: A Study of the Sensitivity of Intra-Aneurysmal Flow Patterns to Flow Conditions in the Carotid Arteries. American Journal of Neuroradiology, 27: 2061-2068, 2006a.

Castro, M.A., Putman, C.M., Cebral, J.R., Patient-specific computational modeling of cerebral aneurysms with multiple avenues of flow from 3D rotational angiography images. *Academic Radiology*, 13:811–821, 2006b.

Castro, M.A., Putman, C.M., Cebral, J.R., Computational Fluid Dynamics Modeling of Intracranial Aneurysms: Effects of Parent Artery Segmentation on Intraaneurysmal Hemodynamics. *American Journal of Neuroradiology*, 27:1703-1709, 2006c.

Castro, M.A., Putman, C.M., Cebral, J.R., Hemodynamic Patterns of Anterior Communicating Artery Aneurysms: A Possible Association with Rupture. *American Journal of Neuroradiology*, 30(2):297-302, 2009a.

Castro, M.A., Putman, C.M., Radaelli, A., Frangi, A., Cebral, J.R., Hemodynamics and rupture of terminal cerebral aneurysms. *Academic Radiology*, 16(19):1201-1207, 2009b.

Cebra,l J.R., Lohner, R., Choyke, P.L., et al., Merging of intersecting triangulations for finite element modeling. *Journal of Biomechanics*, 34:815–819, 2001.

Cebral, J.R., Castro, M.A., Appanaboyina, S., Putman, C., Millán, D., Frangi, A., Efficient Pipeline for Image-Based Patient-Specific Analysis of Cerebral Aneurysms Hemodynamics: Technique and Sensitivity. *IEEE - Transactions on Medical Imaging - Special Issue on Vascular Imaging*, 24(4):457-467, 2005.

Cebral, J.R., Castro, M.A., Putman, C.M., Alperin, N., Flow-area relationship in internal carotid and vertebral arteries. *Physiological Measurements*, 29(10):585-594, 2008.

Cebral, J.R., Sheridan, M., Putman, C.M., Hemodynamics and Bleb Formation in Intracranial Aneurysms. *American Journal of Neuroradiology*, 31:304-310, 2010.

Cebral, J.R., Mut, F., Weir, J., Putman, C.M., Quantitative characterization of the hemodynamic environment in ruptured and unruptured brain aneurysms. *American Journal of Neuroradiology*, 32:145-151, 2011.

Charbel, F.T., Seyfried, D., Metha, B., et al., Dominant A1: angiographic and clinical correlations with anterior communicating artery aneurysms. *Neurological Research*, 13:253–256, 1991.

Crompton, M., Mechanisms of growth and rupture in cerebral berry aneurysms. *British Journal of Medicine*, 1:1138-1142, 1966.

Ford, M.D., Hoi, Y., Piccinelli, M., Antiga, L., Steinman, A.D., An objective approach to digital removal of saccular aneurysms: Technique and applications. *The British Journal of Radiology*, 82:56-61, 2009.

Hashimoto, N., Handa, H., Nagata, I., et al., Experimentally induced cerebral aneurysms in rats. Part V. Relation of hemodynamics in the circle of Willis to formation of aneurysms. *Surgical Neurology*, 13:41–45, 1980.

Horiuchi, T., Tanaka, T., Hongo, K., Surgical treatment for aneurysmal subarachnoid hemorrhage in the 8th and 9th decade of life. *Neurosurgery*, 56:469–475, 2005

Jou, L.D., Lee, D.H., Morsi, H., Mawad, M.E., Wall Shear Stress on Ruptured and Unruptured Intracranial Aneurysms at the Internal Carotid Artery. *American Journal of Neuroradiology*, 29:1761-1767, 2008.

Kasuya, H., Shimizu, T., Nakaya, K., et al., Angles between A1 and A2 segments of the anterior cerebral artery visualized by three-dimensional computed tomographic angiography and association of anterior communicating artery aneurysms. *Neurosurgery*, 45:89–93, 1999.

Kulcsar, Z., Ugron, A., Marosfo, M., Berentei, Z., Paal, G., Szikora, I., Hemodynamics of Cerebral Aneurysm Initiation: The Role of Wall Shear Stress and Spatial Wall Shear Stress Gradient. *American Journal of Neuroradiology*, 32(3):587-594, 2011.

Leipzip, T.J., Morgan, J., Horner, T.G., Analysis of intraoperative rupture in the surgical treatment of 1674 saccular aneurysms. *Neurosurgery*, 56:455–468, 2005.

Löhner, R., Extensions and improvements of the advancing front grid generation technique. *Computational Methods in Applied Mechanical Engineering*, 5:119–132, 1996a.

Löhner, R., Regridding surface triangulations. Journal of Computational Physics, 126:1–10, 1996b.

Löhner, R., Automatic unstructured grid generators. *Finite Elements Analysis Design*. 25:111–134, 1997.

Mazumdar, J.N., Biofluid Mechanics, *World Scientific*, Singapore, 1992.

Nakatani, H., Hashimoto, N., Kang, H., Yamazoe, N., Kikuchi, H., et al., Cerebral blood flow patterns at major vessel bifurcations and aneurysms in rats. *Journal of Neurosurgery*, 74:258-262, 1991.

Perlmutter, D., Rhoton, A.L.J., Microsurgical anatomy of the anterior-anterior communicating-recurrent artery complex. *Journal of Neurosurgery*, 45:259 –272, 1976.

Sherman, T.F. On connecting large vessels to small. The meaning of Murray's law. *J Gen Physiol.*,

78:431–453, 1981.
Shojima, M., et al., Magnitude and role of wall shear stress on cerebral aneurysm. Computational fluid dynamic study of 20 middle cerebral aneurysms. *Stroke*, 35:2500-2505, 2004.
Shojima, M., Nemoto, S., Morita, A., Oshima, M., Watanabe, E., Saito, N., Role of Shear Stress in the Blister Formation of Cerebral Aneurysms. *Neurosurgery*, 67(5):1268-1275, 2010.
Taylor, C.A., Hughes, T.J.R., Zarins, C.K., Finite element modeling of blood flow in arteries. *Computational Methods in Applied Mechanical Engineering*, 158:155–196, 1998.
Womersley, J.R., Method for the calculation of velocity, rate of flow and viscous drag in arteries when the pressure gradient is known. *J Physiol*, 127:553–563, 1955.
Yim, P.J., Vasbinder, B., Ho, V.H., et al., A deformable isosurface and vascular applications. *In: Sonka M and Fitzpatrick JM, ed. Medical Imaging 2002: Image Processing, SPIE Vol. 4684. San Diego, Calif: SPIE*; 1390–1397, 2002.